PAPER

Optimized hydrodynamic interactions in phalanx school arrays of accelerated thunniform swimmers

Physica Scripta

PAPER

Optimized hydrodynamic interactions in phalanx school arrays of accelerated thunniform swimmers

Ahmed Abouhussein and Yulia T Peet

School of Engineering, Matter, Transport and Energy, Arizona State University, Tempe, AZ, 85287, United States of America

E-mail: aabouhus@asu.edu

RECEIVED
27 October 2022

REVISED
16 December 2022

ACCEPTED FOR PUBLICATION
1 February 2023

PUBLISHED
14 February 2023

Keywords: phalanx, fish, propulsion, optimization, CFD, surrogate modelling, acceleration

Abstract

Optimal fish array hydrodynamics in accelerating phalanx schools are investigated through a computational framework which combines high fidelity Computational Fluid Dynamics (CFD) simulations with a gradient free surrogate-based optimization algorithm. Critical parameters relevant to a phalanx fish school, such as midline kinematics, separation distance and phase synchronization, are investigated in light of efficient propulsion during an accelerating fish motion. Results show that the optimal midline kinematics in accelerating phalanx schools resemble those of accelerating solitary swimmers. The optimal separation distance in a phalanx school for thunniform biologically-inspired swimmers is shown to be around $2L$ (where L is the swimmer's total length). Furthermore, separation distance is shown to have a stronger effect, *ceteris paribus*, on the propulsion efficiency of a school when compared to phase synchronization.

1. Introduction

Fish schools are known to provide hydrodynamic benefits to group members when compared to solitary swimming [1–3]. Phalanx schools, in particular, have been investigated through different methods which include self-propelled rigid foils [4], self-propelled flexible foils [5], numerical simulations of undulating swimmers [1, 6], and fish tank experiments [7, 8]. Recent investigations suggest that the phalanx group swimming efficiency is sensitive to the separation distance between swimmers in the school [1, 9, 10], with varying conclusions reached regarding the most beneficial swimming regime with respect to separation distance. For example, Hemelrijk's *et al* [1] investigation of phalanx schools of mullet-shaped fish in steady flow revealed that the propulsive efficiency of the group is higher than a solitary swimmer as long as the separation distance within the school remains greater than or equal to one fish length. When the separation distance is smaller than one fish length, the authors noted that the group's swimming efficiency decreases below that of a steady solitary swimmer [1]. Conversely, Li *et al* [9] notes that phalanx formations of red nose tetra fish have a high average cost of transport when the separation distance is close to one fish length. Instead, from their simulations, a separation distance of roughly half a fish length could provide a 2% improvement in the group's average cost of transport when compared to a solitary swimmer, assuming steady flow [9]. Another study, using an inviscid model, showed that tightly packed phalanx schools of rigid airfoils, with roughly half a chord length of separation distance, show a 5% improvement in the group steady swimming speed, when compared to a single airfoil [10]. This improvement is accompanied, however, by a 4% increase in the average cost of transport over that of a single airfoil. The observed speed-up and a higher cost of transport both decrease as the separation distance between the airfoils is increased until the system eventually approaches the single airfoil limit [10]. The preferred separation distance in a school can depend on a range of different factors such as the swimming speed and/or Reynolds number [8], and the phase difference between swimmers [11]. It remains to be the case, however, that the group propulsive efficiency of fish schools in general, and for phalanx schools in particular, is directly related to the separation distance of swimmers within it.

Phase synchronization was likewise found to be important for phalanx schools, where, e.g. red nose tetra fish showed a preference towards either in-phase or an anti-phase swimming over all other synchronization modes

[7]. Several computational studies of a swimming fish pair demonstrated an increased stability in synchronized configurations [6, 9, 12] (either anti-phase or in-phase). Furthermore, Dewey *et al* [13] observed that side-by-side hydrofoils that oscillate out of phase result in an increased thrust, while in-phase oscillations reduce the total power input.

A different, but nevertheless important, schooling parameter to consider is the swimmers' gait [14]. Previous investigations of phalanx schools using undulating flexible fish-shape bodies rely on a fixed kinematic gait based on empirical data [1, 9, 11], which is often obtained by observing the midline envelope of real fish in steady swimming [7, 15]. However, an optimized kinematic adjustment could result in improved swimming performance through schooling mechanisms such as wake capturing [16]. In fact, for swimmers to only maintain their relative position in a school, kinematic adjustment is required [9]. Additionally, kinematic gaits based on steady state swimming may not necessarily apply to unsteady swimming. Indeed, accelerating swimmers have distinctively different hydrodynamic and kinematic behaviour than steady swimmers. For example, a large survey of over 50 species of real fish revealed that accelerating fish consistently swim with a higher tail amplitude when compared to steady swimming [17]. Similar studies report that eels and bluegill sunfish increase both their tail amplitude and undulation frequency during acceleration when compared to steady swimming [18, 19]. Additionally, investigations of the force field on the body of a robotic tuna-shaped swimmer revealed that during acceleration thunniform swimmers (such as tuna) generate a significant portion of forward thrust using their main body and may, consequently, adopt a more anguilliform-like body motion [20]. While linear acceleration may have been investigated for single swimmers, little is known about the collective behaviour of accelerating phalanx schools and the associated changes in kinematic motion. Accelerating collective motions play an important role in many biological functions of fish schools, such as an escape from predator, and also for the design of efficient maneuvers for autonomous underwater vehicles.

While previous studies looked at the influence of various parameters on schooling performance in isolation, the goal of the current work is to develop a holistic approach to an analysis of the schooling problem that considers a variation of affecting parameters simultaneously, rather than consecutively. This will be accomplished by casting a problem of finding the most beneficial schooling strategy as a formal optimization problem. A discussion of the advantages of using a formal optimization technique over *a priori* (nonrandom or random) sampling can be found in literature [21–23]. In particular, it removes dependence on either an a-priori user knowledge, or a random chance, in identifying 'promising regions', it provides a guarantee that the effective configurations were not missed, and it yields critical information regarding the relative gains between different adaptation strategies. By comparing optimum and sub-optimum configurations, we are able to elucidate on hydrodynamical aspects of efficient schooling and identify physical mechanisms, via which the efficiency enhancement can occur in different schools by contrasting, for example, the adaptation strategies that tend to maximize the useful work (or a group thrust performance) versus minimizing the total work (or the total energy expenditure by the school). Finally, the developed optimization framework allows us to offer a unique perspective regarding the link between stability and efficiency in a collective locomotion, a pressing question that has been demanding answers for quite some time [9, 24, 25].

Formal optimization studies that aim to identify effective schooling configurations from a hydrodynamic perspective are absent in the literature, although works devoted to an optimization of a swimming performance of a solitary swimmer can be noted [14, 23, 26, 27]. Some recent studies also considered the problem of control to ensure that a swimmer can successfully follow a leader on a specified trajectory [16, 28, 29]. The current work does not consider the effects of control, but rather is focused on identifying the hydrodynamically-optimum maintained configurations, which can serve as targets for control strategies. Consequently, in the current study, the relative position between the swimmers is fixed, a framework employed in many recent studies of fish schooling [1, 13, 30–33]. While the swimmers are fixed in place, the effects of destabilization by the resulting fluid forces due to a swimmers' interaction are implicitly taken into account, as such configurations also tend to correlate with high total work, which is penalized in the optimization procedure.

We use our previously developed approach that couples an optimization algorithm to high fidelity spectral CFD simulations [34], to allow for a coupled fish array hydrodynamics to be fully optimized in terms of their midline kinematics, phase difference and undulation frequency. Three phalanx schools, with varying separation distances, are presented to highlight changes in optimal behaviour depending on the compactness of a school. The phalanx setups are also compared to an optimized solitary swimmer to highlight the differences between the school and single fish performance. The rest of the paper is organized as follows. In section 2, we describe the physical and numerical modeling of phalanx swimmers and the optimization cases set-up. Section 3 includes the results of the optimization cases for both solitary and phalanx swimmers. Section 4 contains discussion and interpretation of the results. Lastly, section 5 presents concluding remarks.

2. Methods

2.1. Physical model

The schooling model introduced in the current study employs the following assumptions: (1) Fish relative position in a school is fixed, (2) All fish swim with the same kinematics (albeit different phase angles), (3) Fish self-propulsion is determined by the average of the fluid forces acting on each swimmer, (4) Fish is synchronized in pairs, (5) Fish and schooling geometry are assumed to be two-dimensional. While these assumptions inevitably lose some complexity of realistic fish schools [35–37], they provide a tractable mathematical model to be used in the current optimization study, which nonetheless keeps the essential physics of the problem as exemplified by many recent studies of fish schooling hydrodynamics that employed similar assumptions [1, 13, 30, 31, 33, 38].

The shape and kinematics of swimmers in the phalanx school is modeled using a two-dimensional approximation of a thunniform swimmer in the streamwise-lateral plane. The geometrical features of a single thunniform swimmer are extracted from real fish data [39, 40], which allows us to specify the shape of the symmetric left and right lateral cross-sectional body curves, $y_l^s(x)$, $y_r^s(x)$, at its static configuration [34, 41]. The total dimensional length of a swimmer, L, is chosen to be 0.3 m to mimic the length of a soft robotic thunniform swimmer prototype in the work of [39, 40]. The midline kinematics of each swimmer in the school are described by the traveling wave equation for thunniform swimmers [42, 43]:

$$y_m(x,\ t) = \left[c_0 + c_1\frac{x}{L} + c_2\left(\frac{x}{L}\right)^2\right]\sin(kx - \omega t + \phi), \tag{1}$$

where y and x are the lateral and streamwise coordinates of the midline points, respectively, t is the time variable, L is the fish length, c_0, c_1 and c_2 are the zeroth-order, linear and quadratic wave amplitudes, k is the wave number associated with the body motion, w is the wave frequency, and ϕ is the phase. Biological investigations suggest that thunniform swimming can be characterized by the following body wave number relation [44],

$$k = \frac{2\pi}{\lambda L},$$

where λ, the body wave length, was measured to be ~1.1. Consequently, we fix λ to be 1.1. To find a deformed fish position at each time, we first compute the position of the midline from equation (1), and then we reconstruct the lateral surfaces $y_l(x, t)$, $y_r(x, t)$ by shifting the cross-sectional segments orthogonal to the midline while approximately conserving the body volume [34, 45].

Self-propulsion is modeled by considering Newton's second law of motion for undulating swimmers, while calculating the corresponding viscous and pressure forces directly from the fully-resolved simulations of the fluid-body interactions:

$$m\ \frac{d\ U(t)}{dt} = \langle F_x(t)\rangle, \tag{2}$$

where m is the mass of the fish, $U(t)$ is the fish forward velocity and $\langle F_x(t)\rangle$ is the streamwise self-propelling force acting on the swimmers averaged among the school members. This array-averaged force $\langle F_x(t)\rangle$ is defined as

$$\langle F_x(t)\rangle = \frac{1}{N}\sum_{k=1}^{N}\oint_{\Gamma_k} -(\sigma_k\ \mathbf{n}_k)\cdot\mathbf{i}\ d\ \Gamma, \tag{3}$$

where σ_k is the total fluid stress tensor acting on the surface of the swimmer k, which includes viscous and pressure contributions, Γ_k is the curvilinear boundary of the swimmer k, $\mathbf{n}_k$ is the outer surface normal of the swimmer k, $\mathbf{i}$ is the unit vector in the streamwise direction, and N is the number of swimmers. Only the contribution of the streamwise force, $\langle F_x(t)\rangle$, i.e. thrust and drag, is considered in the propulsion law of equation (2), and thereby the swimmer(s) are confined to move in the streamwise direction and do not travel in the lateral direction. Similar assumptions were made in previous studies of both single and collective swimming [31, 34, 46]. Taking the propulsion force for each swimmer to be an array-averaged force and restricting it to a streamwise direction allows us to keep the streamwise and lateral separation distances, and the direction of motion, fixed within the array, so that the specified phalanx geometries during a linear accelerating motion could be studied.

2.2. Numerical model

The numerical modeling in the current study follows the method previously developed and validated in [34]. Fluid-body interactions of the modeled swimmer are solved by considering the Arbitrary Lagrangian-Eulerian (ALE) formulation of the incompressible Navier–Stokes (NS) equation on a moving mesh [34, 47, 48]:

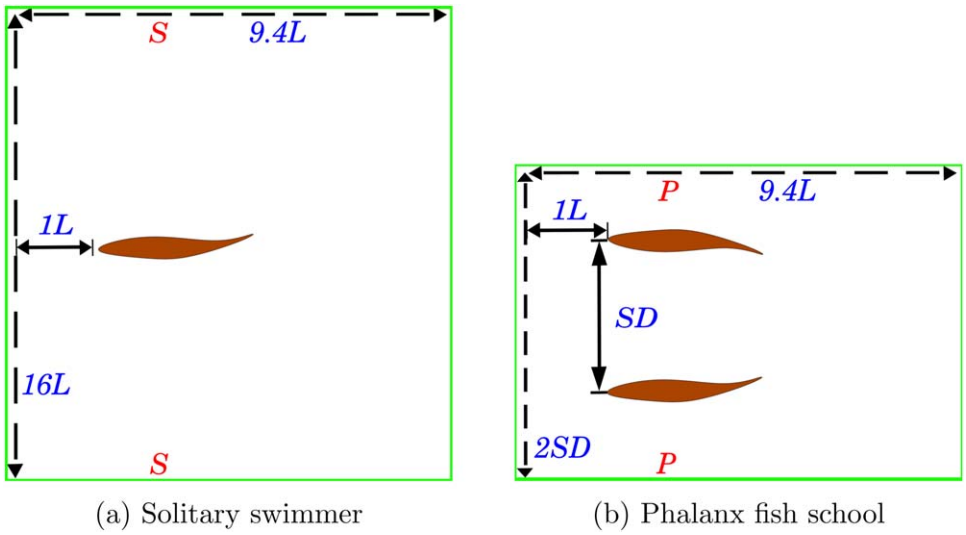

Figure 1. A schematic of the computational domain for (a) Solitary swimmer, (b) Phalanx fish school. 'S' stands for symmetry, 'P' stands for periodicity in lateral boundary conditions.

$$\rho\left(\frac{\delta \mathbf{u}}{\delta t} + (\mathbf{u} - \mathbf{w}) \cdot \nabla \mathbf{u}\right) + \nabla p = \mu \Delta \mathbf{u}, \tag{4a}$$

$$\nabla \cdot \mathbf{u} = 0, \tag{4b}$$

where ρ, $\mathbf{u} = \{u_x, u_y\}$, p, μ and $\mathbf{w} = \{w_x, w_y\}$ are the fluid density, velocity, pressure, dynamic viscosity and the mesh velocity, respectively, while the derivative $\delta/\delta\, t$ represents the ALE derivative. A high-order spectral element method (SEM) [48, 49] is used to solve the NS equations. In the SEM, a body-fitted element mesh is constructed, and the solution within each element is represented by tensor-product polynomial functions defined on a set of Gauss-Lobatto-Legendre (GLL) integration nodes [48, 49].

The Newton's propulsion law (equation (2)) is advanced implicitly by using the backward Euler scheme as

$$U^n = U^{n-1} + \frac{\delta t}{m}\langle F_x^n \rangle, \tag{5}$$

where δt is the time step and $\langle F_x^n \rangle = \langle F_x(t^n) \rangle$ is the propelling force acting on the swimmer(s) in the x direction at a time t^n. Implicit update is accomplished via fixed-point iteration with Aitken relaxation [50] and typically converges in 3–4 iterations to a set tolerance of 1×10^{-4}. Implicit treatment of the Newton's propulsion law is necessary to avoid the added mass instabilities pertinent to incompressible fluid-structure interaction problems [51, 52]. Further details regarding the numerical methodology in the context of modeling of self-propelled biological swimmers are found in [34]. The fluid and fish density are both taken to be $1 \times 10^3\,\mathrm{kg/m^3}$, which corresponds to a neutrally-buoyant swimmer. Dynamic viscosity of the fluid, μ, is set to $1 \times 10^{-3}\,\mathrm{kg/(m \cdot s)}$. The mass of each swimmer m is specified as 0.8606 kg, which corresponds to the parameters of a soft robotic thunniform swimmer prototype [40].

The computational domain for the solitary swimmer and for the phalanx school simulations is presented in figure 1. For the solitary swimmer, the computational domain is a rectangle with dimensions $9.4L \times 16L$, with the fish placed in the center of the domain and $1L$ away from the inlet. To simulate an infinite phalanx array, we include two fish into the domain separated by the distance SD while accounting for the remaining fish via periodicity in the lateral direction. The streamwise extent of the phalanx domain is the same as in the solitary case, leading to a size of $9.4L \times 2SD$, with the leading edge of the fish array located, again, at $1L$ from the inlet, see figure 1. Note that while periodic array simulations are possible with a single swimmer in the domain [53], inclusion of at least two swimmers is required to study the effect of a phase lag. Thus, in the current setup, we fix the phase of the left swimmer at $\phi = 0$, while the phase ϕ of the right swimmer represents the phase lag. For a single swimmer, a phase $\phi = 0$ is used. Consequently, we specify $N = 1$ for a single swimmer, and $N = 2$ for the school in equation (3).

We set the GLL node count as $N_x = N_y = 7$, leading to the 6th order of the basis interpolating polynomial functions. Fluid velocity at the fluid-body interface (surfaces $y_l(x, t)$, $y_r(x, t)$) is set equal to the velocity of the moving boundary, which is obtained from differentiating the corresponding equations for $y_l(x, t)$, $y_r(x, t)$ in time (See [34] for more details). A self-propulsion is handled by keeping the fish geometrical position fixed while adjusting the inlet velocity at a time step t^n to be equal to the self-propulsion velocity U^n obtained from equation (5). A pressure outflow boundary is used at the outlet. Symmetry conditions are used at the lateral

boundaries for a solitary swimmer, while periodicity conditions are used at the lateral boundaries in the phalanx schools to simulate an infinite array of swimmers. During the initial phase of the simulations, the fish and the corresponding SEM mesh are deformed from their static configuration to the one corresponding to a midline position of equation (1) evaluated at $t = 0$ as described in [34].

2.3. Optimization

The general optimization problem is stated as

$$\begin{aligned} &\text{maximize} \quad f(\mathbf{z}) \\ &\text{subject to} \quad \mathbf{z} \in \mathbb{R}^n, \end{aligned} \tag{6}$$

where $f\colon \mathbb{R}^n \to \mathbb{R}$ is the objective function, and $\mathbf{z} \in S \cap C$ is a vector of design parameters. The set $S \subseteq \mathbb{R}^n$ contains the n-dimensional search space and the set $C \subseteq \mathbb{R}^n$ contains a set of $m \geqslant 0$ inequality constraints, as presented in [34, 54]. In the current work, the traveling wave amplitude coefficients, that is $\{c_0, c_1, c_2\}$, the undulation frequency f, and the phase lag ϕ make up the design parameters, $\mathbf{z} = \{c_0, c_1, c_2, f, \phi\}$. For a solitary swimmer, the design parameter ϕ is omitted. We restrict ourselves to a situation where all swimmers in a phalanx school have the same kinematics (i.e. amplitude coefficients and undulation frequency), which justifies the definition of averaged quantities within a school, such as in equation (3).

The set, S is given by:

$$\begin{aligned} -0.0500L \leqslant c_0 \leqslant 0.0500L, \\ -0.1000L \leqslant c_1 \leqslant 0.8333L, \\ -0.7333L \leqslant c_2 \leqslant 0L, \\ 0 \leqslant f \leqslant 3, \\ 0 \leqslant \phi \leqslant 2\pi, \end{aligned} \tag{7}$$

with the 5th equation omitted for a solitary swimmer. In order to allow for only physically realizable modes as deduced from biological data, the following constraint set, C, is imposed [39, 40, 46]:

$$\begin{aligned} g_1(\mathbf{x}) &= c_0 + c_1 + c_2 - 0.1L \leqslant 0, \\ g_2(\mathbf{x}) &= -c_0 - c_1 - c_2 - 0.1L \leqslant 0, \\ g_3(\mathbf{x}) &= c_0 - \frac{c_1^2}{4c_2} - 0.1L \leqslant 0, \\ g_4(\mathbf{x}) &= -c_0 + \frac{c_1^2}{4c_2} - 0.1L \leqslant 0. \end{aligned} \tag{8}$$

The first two constraints ensure that the tail amplitude does not exceed 0.1 L, while the last two constraints restrict the maximum body undulation to under 0.1 L.

The group propulsive efficiency, η, is taken to be the objective function, $f(\mathbf{z})$. The group propulsive efficiency is defined as the ratio of a collective 'useful' energy gained, over the total collective work done by the swimmers over a certain time period, which can be stated as

$$\begin{aligned} \eta(c_0, c_1, c_2, f, \phi) &= \frac{W_{\text{useful}}}{W_{\text{total}}} \\ &= \frac{\sum_{k=1}^{N} \int_0^{2T} \left(\oint_{\Gamma_k} -(\sigma_k \mathbf{n}_k) \cdot \mathbf{i} \, d\Gamma \right) U(t) dt}{\sum_{k=1}^{N} \int_0^{2T} \left(\oint_{\Gamma_k} -(\sigma_k \mathbf{n}_k) \cdot \mathbf{v}_k(x, y, t) \, d\Gamma \right) dt} \end{aligned} \tag{9}$$

where $T = 1s$ and $\mathbf{v}_k(x, y, t)$ is the swimmer's k surface velocity due to undulation. By describing η as the ratio of W_{useful} to W_{total}, the current optimization problem is regarded as a multi-objective optimization problem with $f(\mathbf{z})$ being a 'weighted product' scalarized utility function [55]. Recall that $N = 2$ in the current setup for the phalanx school, and $N = 1$ for the solitary swimmer. Under $N = 1$, equation (9) reduces to a traditional definition of a single swimmer propulsive efficiency found in [17, 34, 56, 57].

A total of four optimization cases are considered to represent three phalanx schools and a solitary swimmer. The phalanx school cases only differ in respect to the separation distance SD, which is varied between $1L$, $2L$ and $3L$, respectively. The optimization cases are solved with a surrogate based optimization (SBO) algorithm that has been shown to be well suited for constrained engineering problems [34, 54]. 30 data points are chosen to construct the initial surrogate for all cases using the Latin Hypercube Sampling method [58]. Additionally, the maximum iteration count $k_{\max}$, and the tolerance termination criterion for the optimization procedure $\varkappa_{\text{opt}}$ [34] are set to 1000 and 1×10^{-3}, respectively.

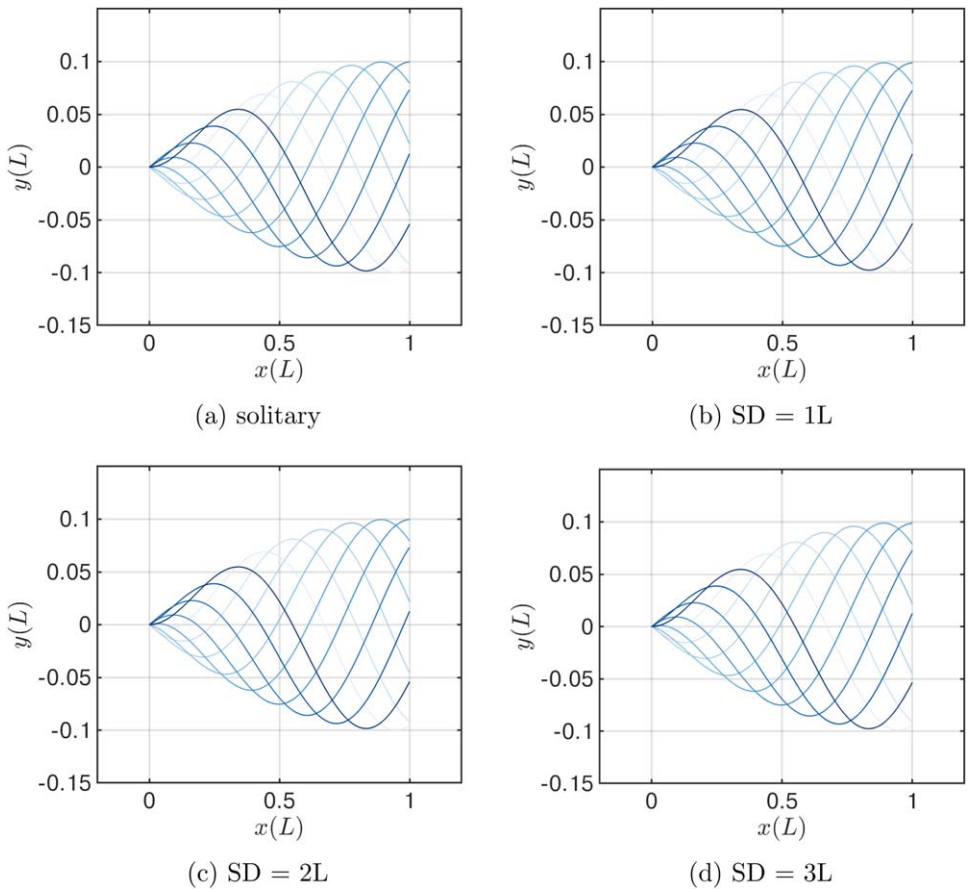

Figure 2. Swimmer midline deformation across one period for four optimum propulsive modes: (a) solitary; (b) SD = 1L; (c) SD = 2L; and (d) SD = 3L. Deformations of the midline in time are encoded every 1/10th of the period in the different shades of blue from lightest ($t = 0$) to darkest ($t = 1/3$).

Table 1. Optimization results.

Case	Evaluations	Optimal parameter set	Efficiency	Tolerance
SD = 1L	51	$\{0.0001L, 0.2096L, -0.1107L, 3, 1.037\pi\}$	21.49%	4.8×10^{-4}
SD = 2L	42	$\{0.0L, 0.2105L, -0.1107L, 3, 0.9995\pi\}$	22.05%	9.9×10^{-4}
SD = 3L	39	$\{-0.0001L, 0.2104L, -0.1108L, 2.9998, 0.9613\pi\}$	21.83%	2.4×10^{-4}
solitary	34	$\{0.0L, 0.2105L, -0.1107L, 3\}$	21.73%	4.0×10^{-4}

3. Results

3.1. Optimization results

Table 1 presents the optimization results for all the cases, which include the number of evaluations, tolerance at termination, optimal parameters, and efficiency. It can be appreciated that all cases terminated within the tolerance, with total evaluation counts that are significantly below the maximum iteration count $k_{\max}$. The number of evaluations ranged from 34 to 51 evaluations, with the first 30 coming from the initial sampling scheme and 4–21 optimization iterations. The first three parameters related to midline deformations, namely $\{c_0, c_1, c_2\}$, are found to be closely similar to that of the optimum solitary swimmer. In other words, all three fish pair cases report similar optimum kinematics to that of a solitary swimmer (figure 2). These kinematics show no noticeable head motion, along with growing body undulations to reach a tail amplitude of roughly $0.1L$. The $0.1L$ is the maximum allowable tail amplitude according to the present constraints (equation (8)). Similarly, the optimum undulation frequency remains close to the upper bound of 3 Hz for the three schools. These results are in agreement with the postulated high-efficiency adaptations deduced from biological data [17, 59]. The optimum phase lag parameter, ϕ, is shown to be close to π, which represents an anti-phase lag between swimmers in an infinite array of a phalanx fish school, consistent with the previous literature [6, 7]. The vorticity

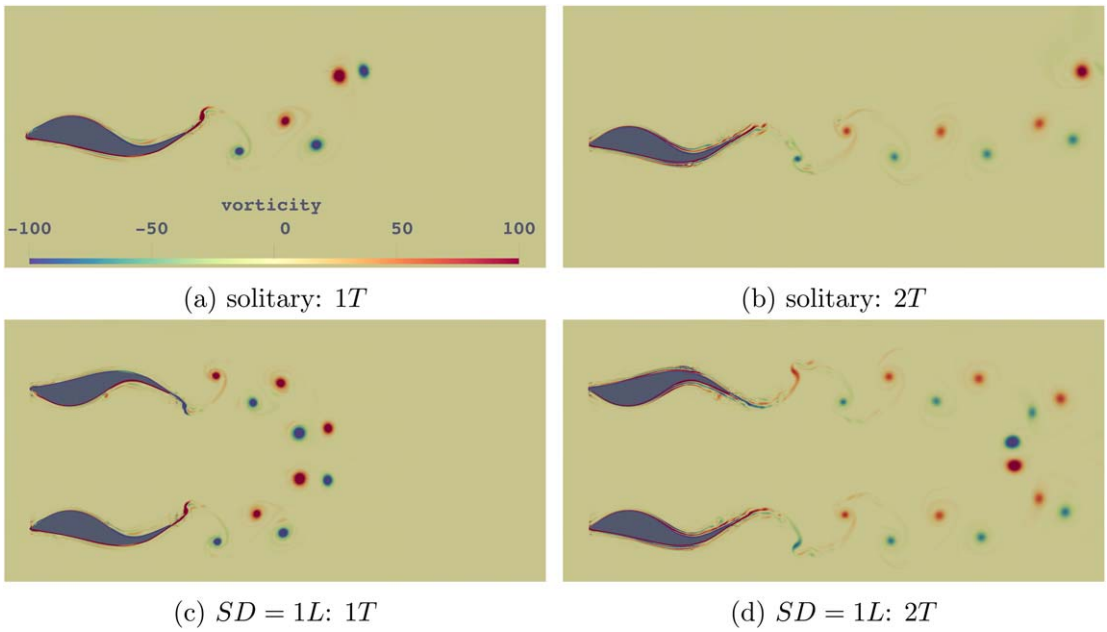

Figure 3. Vorticity (color bar shown in solitary: $1T$ subfigure) in the wake of the swimmers for the optimum mode in solitary swimming (top row) and the $SD = 1L$ phalanx school (bottom row) after $1T$ (left) and $2T$ (right), respectively ($T = 1s$).

Table 2. Optimization results for phalanx schools at $SD = 2L$ using 2 and 3 simulated swimmers.

Number of swimmers	Evaluations	Optimal parameter set	Efficiency	Tolerance
2	42	$\{0.0L, 0.2105L, -0.1107L, 3, 0.9995\pi\}$	22.05%	9.9×10^{-4}
3	74	$\{0.0062L, 0.1882L, -0.0945L, 3, 1.0583\pi, 0\}$	22.06%	3.8×10^{-4}

field created by the solitary and $SD = 1L$ optimum swimming modes is shown after $1T$ and $2T$ in figure 3. The wakes behind optimum swimmers are quite similar to the reverse von Karman street typically associated with high propulsive swimming efficiency in real fish [60], with no significant interactions noted between the wakes of swimmers in the phalanx school at this separation.

To assess the sensitivity of the optimization results to a number of simulated swimmers in a periodic domain, we perform another optimization study for a phalanx school with 3 simulated swimmers at $SD = 2L$. In this case, the design vector, $\mathbf{z} = \{c_0, c_1, c_2, f, \phi, \phi'\}$, is 6th dimensional and accounts for the phase lag of the third swimmer, ϕ' (both ϕ and ϕ' are taken as the phase difference in relation to the first, or the leftmost, swimmer). Results of the 3-swimmer optimization case, shown in table 2, do not significantly deviate from its 2-swimmer counterpart, suggesting that the current optimization results are insensitive to the number of simulated swimmers. In the rest of the paper, we present results from the baseline case that contains 2 swimmers in the domain.

The reported optimum efficiency is slightly different for each fish school, where the highest reported efficiency, $\eta^*_{2L} = 22.05\%$, is found at a separation distance of 2L. The dense school ($SD = 1L$) and the sparse school ($SD = 3L$) report lower optimum efficiencies of $\eta^*_{1L} = 21.49\%$ and $\eta^*_{3L} = 21.83\%$, respectively. In contrast to a solitary swimmer, we observe that phalanx fish schools with $SD = 2L$ ($\frac{\eta^*_{2L} - \eta^*_s}{\eta^*_s} \approx 1.5\%$) and $SD = 3L$ ($\frac{\eta^*_{3L} - \eta^*_s}{\eta^*_s} \approx 0.5\%$) are slightly more efficient, while the $SD = 1L$ school ($\frac{\eta^*_{1L} - \eta^*_s}{\eta^*_s} \approx -1.1\%$) is slightly less efficient. While the observed increase in efficiency of the most optimal phalanx school is slight (1.5%), the schooling efficiency depends on a range of factors, which include the Reynolds number [60], the swimmer's shape [27], and the undulation frequency [14, 61]. Another important consideration is the definition of efficiency itself, which varies among the studies. In this work, we consider the propulsive efficiency, which is the product of the net force and the forward velocity divided by the input power (equation (9)), relevant for the characterization of acceleration due to propulsion [17]. Nevertheless, when we compare the estimated increase in the current study with some other efficiency metrics in the literature, we see that the current observed increase in efficiency does not significantly deviate from previously reported values. For example, [9] use a 'Cost of

Transport' (CoT) as a measure of propulsive efficiency during steady swimming and report a 2% improvement in the CoT of a phalanx school when compared to solitary swimming. The authors of [1], using a modified version of the Froude efficiency, report an approximately 3% increase of efficiency in steady phalanx schools when compared to solitary swimming.

3-D stem plots of optimization cases are shown in figure 4. 3-D space is used to represent each data point according to its respective parameter value and is colored by its respective propulsive efficiency value. Consequently, multiple stem plots are presented for each case to account for all four and five dimensions for solitary and school swimming, respectively.

For the phalanx school cases, data points with the highest efficiencies are located within the same region of the 3-D space in each stem plot. This optimal efficiency region is characterized by a small head motion ($c_0 \approx 0$), a high frequency ($f \approx 3$ Hz) and a phase lag, $\phi = \pi$, commonly referred to as anti-phase swimming. In other words, efficient swimming patterns in all three phalanx schools rarely deviated from the configuration suggested by their respective optimum mode.

We define the maximum attainable swimming speed at the end of the considered period 2 T as $U_{\max} = U(t = 2\ T)$. Additionally, we define the time-averaged array-averaged streamwise force $\bar{F}_x$ acting on the swimmer:

$$\bar{F}_x = \frac{1}{t_0}\int_0^{t_0} \langle F_x(t)\rangle\ d\ t \tag{10}$$

with $t_0 = 2\ T$. Table 3 presents hydrodynamic quantities such as W_{useful}, W_{total}, $\bar{F}_x$, $U_{\max}$, and the Reynolds number at the maximum speed $Re_{\max}$, defined as:

$$Re_{\max} = \frac{U_{\max} L}{\nu} \tag{11}$$

where $\nu = 1 \times 10^{-6}$ (m^2/s) is the kinematic viscosity of water.

4. Discussion

4.1. Effects of body kinematics on the propulsive efficiency of a solitary swimmer

The optimum undulation of a solitary thunniform swimmer, shown in figure 2, differs slightly from the reported midline kinematics for non-accelerated solitary thunniform swimmers [62, 63]. While in both cases there is no significant head motion, the case presented here shows growing body and tail undulations, while thunniform swimmers in steady motion maintain a relatively straight body and only use their tail for propulsion [63, 64]. The differences are attributed to the effect of acceleration. Indeed, most previous studies [62–66] focus on steady thunniform swimming, with unsteady swimming trends gaining traction only recently. For example, one previous study investigated the acceleration of a solitary thunniform swimmer from rest [20]. Investigation of the pressure forces around a solitary accelerating robotic tuna suggests that the posterior main body generates a significant portion of forward thrust as adjacent fluid is pushed backwards. This mechanism is similar to drag-based propulsion mechanisms found in anguilliform swimming and in low-Reynolds number swimming [67, 68], and hence the study suggests that thunniform swimmers may adopt an anguilliform-like motion as they accelerate from rest, as being more efficient in low speeds. Indeed, current optimization results are in line with this trend, with the optimal point falling in an optimum region in the $c_0 - c_1 - c_2$ space which is characterized by large posterior body and tail undulations (see figure 2). A stronger head yaw was also attributed to acceleration in the studies of anguilliform and carangiform species [17–19]. However, in the studies of accelerating tuna fish, while the increased head amplitude was also observed, it did not appear to generate thrust [20]. It is possible that a stronger head motion during acceleration is not directly driven by efficiency, but by other physiological considerations (for example, it might be easier to produce a high tail amplitude while also moving a head due to muscular constraints), a point that needs to be investigated in the future.

4.2. Effects of body kinematics on the propulsive efficiency of phalanx schools

To understand the similarity in the optimum body kinematics between all three phalanx schools and the solitary swimmer, the main energy saving mechanisms in phalanx fish schools are discussed, namely: channeling and pulsating jet effects. When swimmers in a phalanx school are within close laterally proximity to one another, an area of augmented flow develops between them. This augmented flow arises as a result of each swimmer generating a velocity field in its swimming direction due to the no-slip condition. Since the augmented velocity field imparts momentum in the swimming direction, swimmers need less thrust force to reach a specific swimming speed [53]. This is typically referred to as the channeling effect [69] and can be observed in fish schools which range from phalanx [8] to rectangular [53] and diamond [38] schools. When swimmers in a phalanx school swim with an anti-phase motion, counter rotating vortices are shed by the two neighbors in each

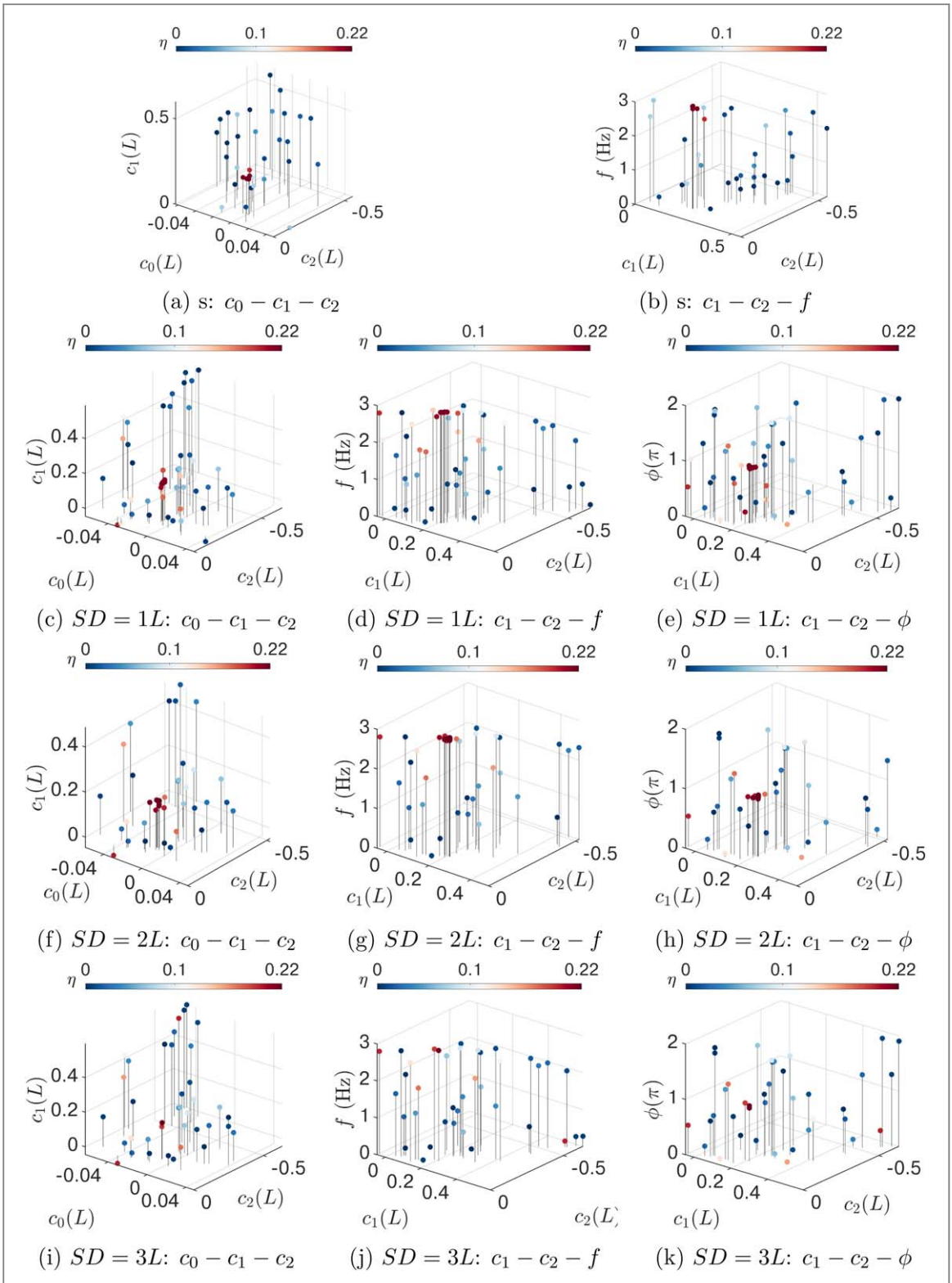

Figure 4. 3-D stem plots of the four dimensions for a solitary swimmer (first row) and five dimensions for phalanx schools with $SD = 1L$ (second row), $SD = 2L$ (third row) and $SD = 3L$ (fourth row).

Table 3. Hydrodynamic quantities of optimum swimmers.

Case	W_{useful} (mJ)	W_{total} (mJ)	$\bar{F}_x$ (N)	$U_{\max}$(m/s)	$Re_{\max}$
SD = 1L	184.11	856.67	0.28139	0.65205	1.96×10^5
SD = 2L	183.69	833.97	0.28108	0.65127	1.95×10^5
SD = 3L	181.78	832.64	0.27961	0.64779	1.94×10^5
solitary	181.19	833.68	0.27916	0.64899	1.95×10^5

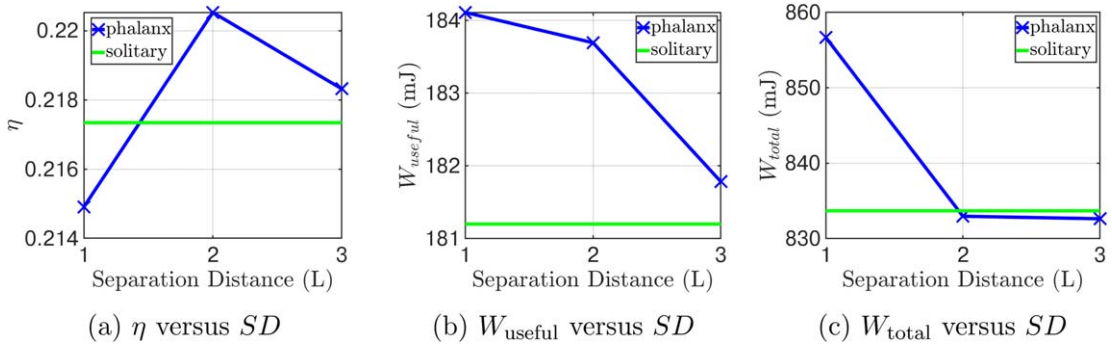

Figure 5. Optimum efficiency, W_{useful} and W_{total} as a function of separation distance within an infinite phalanx school.

half period. These counter rotating vortices combine to form dipoles, producing a pulsating jet behind the swimmers [5]. While in phase swimmers can similarly benefit from the pulsating jet affect, anti-phase swimmers produce higher thrust by creating a more compact jet [5]. Therefore, it can be observed that swimming with a higher undulation frequency will enhance both energy saving mechanisms, since higher undulation frequency will result in faster flow around each swimmer [20] as well as a higher intensity pulsating jet in their wake. Similarly, high body and tail amplitudes result in faster flow and larger vortices, inducing faster propulsion [34]. It is then of no surprise that the optimal midline kinematics in an accelerating phalanx school exhibit similar behaviour to that of a solitary swimmer, achieving a maximized tail displacement as well as an undulation frequency.

4.3. Effects of separation distance on the propulsive efficiency of phalanx schools

Figure 5 shows plots of the optimal propulsive efficiency of each fish school optimization case as a function of the separation distance within a school (Subplot 5(a)). Additionally, the two quantities related to the useful and total work, namely W_{useful} and W_{total}, are included to investigate what is driving the changes in efficiency across different separation distances. As previously noted, the optimal efficiency of a phalanx school in the current study peaks at a separation distance of $2L$ with a value of 22.05%, which amounts to a 1.5% increase over the solitary swimmer optimum. This increase is largely driven by a higher useful work quantity $\frac{W_{\text{useful}_{2L}} - W_{\text{useful}_s}}{W_{\text{useful}_s}} \approx 1.4\%$. The relative change in total work is $\frac{W_{\text{total}_{2L}} - W_{\text{total}_s}}{W_{\text{total}_s}} \approx 0.03\%$, which is an order of magnitude lower than the relative change in W_{useful}. Since the optimum mode uses an anti-phase gait, the increased W_{useful} could likely be attributed to the presence of a pulsating jet behind the swimmers. The presence of a pulsating jet behind the swimmers would increase their time-averaged streamwise force, $\bar{F}_x$ (as seen in table 3), and consequently contribute to more work in the swimming direction or W_{useful}. Indeed, W_{useful} is shown to increase with a decreasing separation distance across the three schools which all employ the same midline and phase kinematics, and is above solitary for all cases. This trend suggests that the increase in W_{useful} is directly related to thrust enhancing mechanisms, such as the pulsating jet and channeling effects, in the phalanx school.

While the school with a $SD = 1L$ results in the highest W_{useful}, its propulsive efficiency is the lowest, even when compared to a solitary swimmer. This happens because W_{total} similarly increases to reach the highest value between all phalanx schools and the solitary swimmer. Since the direction of swimming and the separation distance is fixed within each school (in a sense that the swimmers are not free to drift apart under the influence of fluid forces), swimmers in a school would have to exert additional effort, if needed, to maintain the same fixed distance during swimming. While this may not present a challenge at more sparse schools, such as $SD = 2L$ and $SD = 3L$, this can result in an increased W_{total} in dense schools ($SD \leqslant 1L$). Indeed, the challenge of dense phalanx schools has been investigated in previous studies. For example, Hemerijk *et al* observed a deteriorated steady group swimming efficiency, when compared to solitary swimming, for simulated mullets in phalanx schools with $SD < 1L$ [1]. The authors comment: 'This is probably due to an increased resistance (on average per fish) of the phalanx to oncoming flow due to close proximity of lateral neighbours'. Gazolla *et al* [6] performed simulations, using a vortex particle method, of multiple phalanx schools consisting of pairs of 2-D self-propelled anguilliform swimmers. In these simulations, where swimmers were free to move in both streamwise and lateral directions and only their undulation was fixed, the pairs in a phalanx school diverged after 8 periods. In a bigger phalanx school (consisting of 5 members), the swimmers diverged at an earlier time of 6 periods [6]. Both these studies suggest that swimming in an infinite phalanx school requires active adjustment and added effort to maintain a fixed separation distance, or at the least cohesion, within a school. Inviscid models of rigid wings in

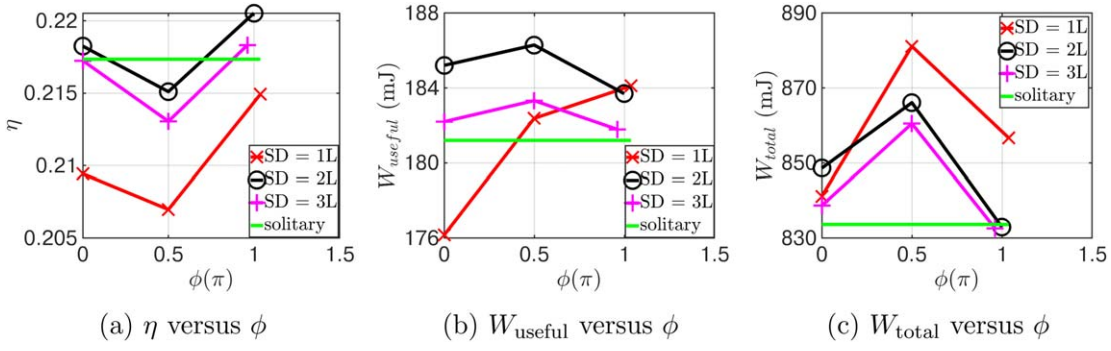

(a) η versus ϕ (b) W_{useful} versus ϕ (c) W_{total} versus ϕ

Figure 6. Optimum efficiency, W_{useful} and W_{total} as a function of phase lag and separation distance within an infinite phalanx school.

steady flow similarly suggest that while densely packed phalanx schools ($SD = 0.66L$) show an 5% increase in the swimming speed over a solitary swimmer (similar qualitative trends can be observed for $U_{\max}$ in table 3), the associated cost of transport increases by 4% [10]. Highly compact schools ($SD < 1L$) could not be simulated here due to computational constraints of the body-fitted CFD methodology. Nonetheless, they represent an important and potentially beneficial case for fish schooling, and they will be included into optimization studies in our future work.

Finally, the most sparse school ($SD = 3L$) displayed similar propulsive trends to the solitary swimmer, where the η, W_{useful} and W_{total} quantities remained relatively unchanged. This is unsurprising, since all the hydrodynamic quantities are expected to approach the solitary swimmer limit with increasing separation distance within a school [10]. The presented optimization cases at different separation distances suggest the presence of three schooling regimes of accelerating phalanx thunniform swimmers:

(i) $SD \leqslant 1L$: higher thrust, higher W_{useful} but higher W_{total} in a phalanx school can be achieved compared to solitary swimming. Consequently, propulsive efficiency could suffer in a dense school.

(ii)$SD \approx 2L$: improved thrust, improved W_{useful} and relatively constant W_{total} compared to solitary swimming. Highest gains in efficiency, when compared to a solitary swimmer, as the school benefits from energy saving mechanisms without providing additional work to maintain its position.

(iii)
$SD \geqslant 3L$: relatively constant thrust, W_{useful}, W_{total} and η as compared to solitary swimming as the school begins to approach the solitary swimmer limit.

4.4. Effects of phase synchronization on the propulsive efficiency of a phalanx school

To isolate the effects of phase synchronization, we compare the optimal point, in each case, to two other points where all other kinematics $\{c_0, c_1, c_2, f\}$ are fixed to optimum values and the phase is changed to 0 and 0.5π, respectively, as shown in figure 6 (note that the phase angles larger than π would result in repeated efficiency points due to symmetry). Between all three schools, anti-phase motion ($\phi = \phi^* \approx \pi$) consistently shows the best swimming efficiency, with the in-phase motion ($\phi = 0$) being second best and the $\phi = 0.5\pi$ being the worst. This is in line with previous studies which investigated phase synchronization behaviour in steady swimming of self-propelled foils. For example, Raspa, Godoy-Diana and Thiria [4] showed that in-phase motion (resulting in asymmetric flow) leads to higher transverse velocity fluctuations, when compared to a motion which results in symmetric flow (arising from anti-phase swimming). As a result, for a given momentum input, the anti-phase motion generated more thrust. A similar study with flexible foils showed that while in-phase motion did benefit swimmers from the pulsating jet effect, it resulted in a wake where the average propulsive jet was more laterally spread, when compared to the wake of an anti-phase motion, and thus did not contribute efficiently to propulsion [5]. This effect was also observed for pairs of real fish in steady swimming [7] where there was a slight preference for anti-phase motion over in-phase. Additionally, a preference of anti-phase and in-phase motion over an intermediate phase lag (such as $\phi = 0.5\pi$) has been previously shown in steady swimming simulations of tetra fish [9].

In the $SD = 2L$ and $SD = 3L$ schools, the most efficient phase lag does not necessarily result in high W_{useful}, indeed it is the lowest for $\phi = \phi^*$, when compared to other ϕ values. Instead, the most efficient phase lag reduces the W_{total} for the school. This is in agreement with the results of Dewey *et al* [13] who observed that for hydrofoils oscillating side by side, an increased efficiency could be attained either by an increase in thrust (as in in-phase oscillations), or by reduction in a total power input (as in anti-phase oscillations). Accordingly, a phase lag of

Table 4. Net streamwise and lateral forces of optimum and sub-optimum swimmers.

Case	$\Delta\bar{F}_{\parallel}\vert_{\phi^*}$(N)	$\Delta\bar{F}_{\parallel}\vert_0$(N)	$\Delta\bar{F}_{\parallel}\vert_{0.5\pi}$(N)	$\Delta\bar{F}_{\perp}\vert_{\phi^*}$(N)	$\Delta\bar{F}_{\perp}\vert_0$(N)	$\Delta\bar{F}_{\perp}\vert_{0.5\pi}$(N)
SD = 1L	0.0409	-5.78×10^{-4}	−0.368	1.171	−0.005	0.861
SD = 2L	4.00×10^{-4}	5.64×10^{-4}	−0.115	0.951	0.002	0.699
SD = 3L	−0.006	-7.944×10^{-5}	−0.067	0.911	0.001	0.657

$\phi = 0.5\pi$ results in the highest W_{total} for all the cases, perhaps due to a complete lack of synchronization and thus even more chaotic flow conditions detrimental for stability. Alternatively, the most efficient phase in the $SD = 1L$ school results in the highest W_{useful} while keeping relatively low W_{total}. This is likely due to phase synchronization effects playing a larger role in dense schools, when compared to sparse schools, and can be further explored in a future study.

Finally, we observe that the relative ranking of efficiency based on separation distance within a school does not change regardless of phase lag, with the most preferable distance remaining $SD = 2L$. Furthermore, it can be seen that higher efficiency gains can be attained by varying the separation distance rather than the phase angle in the school. This suggests that the separation distance within a phalanx school plays a larger role in the schooling efficiency than phase synchronization, for the parameters explored in this study.

4.5. Analysis of swimming stability using differences in the net streamwise and lateral forces

The swimming stability of phalanx swimmers is analyzed by calculating the differences in the net streamwise and lateral forces between swimmers in each phalanx school, a similar process to [9]. We define the difference in the time-averaged net streamwise force, $\Delta\bar{F}_{\parallel}$, as

$$\Delta\bar{F}_{\parallel} = \frac{1}{t_0}\int_0^{t_0} F_1(t)_{\parallel} - F_2(t)_{\parallel}\, d\, t, \tag{12}$$

where $F_1(t)_{\parallel}$ and $F_2(t)_{\parallel}$ are the propulsive (streamwise) forces on the left and right swimmers, defined as

$$F_k(t)_{\parallel} = \oint_{\Gamma_k} -(\sigma_k\, \mathbf{n}_k)\cdot \mathbf{i}\, d\, \Gamma, \tag{13}$$

where $\mathbf{i}$ is the unit vector in the streamwise direction, and $k = 1,2$ correspond to the left and right swimmers, respectively. Similarly, we define the difference in the time-averaged net lateral force, $\Delta\bar{F}_{\perp}$, as

$$\Delta\bar{F}_{\perp} = \frac{1}{t_0}\int_0^{t_0} F_1(t)_{\perp} - F_2(t)_{\perp}\, d\, t, \tag{14}$$

where $F_1(t)_{\perp}$ and $F_2(t)_{\perp}$ are the lateral forces on the left and right swimmers, given as

$$F_k(t)_{\perp} = \oint_{\Gamma_k} -(\sigma_k\, \mathbf{n}_k)\cdot \mathbf{j}\, d\, \Gamma, \tag{15}$$

and $\mathbf{j}$ being the unit vector in the lateral direction. Table 4 includes $\Delta\bar{F}_{\parallel}$ and $\Delta\bar{F}_{\perp}$ for the optimum phalanx swimmers denoted by the phase angle ϕ^* at $SD = 1L$, $2L$, $3L$, as well as the corresponding values for the same kinematics but a phase lag of $\phi = 0$ and $\phi = 0.5\pi$. Using the first row of table 4 as an example: $\Delta\bar{F}_{\parallel}\vert_{\phi^*}$ is the net streamwise force in the optimum school when $SD = 1L$, while $\Delta\bar{F}_{\parallel}\vert_0$(N) is the net streamwise force for a $SD = 1L$ school employing the same optimum body kinematics but with no phase lag between swimmers.

We observe that the optimal school with the smallest separation distance ($SD = 1L$) experiences the largest magnitude of the difference in the net streamwise force or $\Delta\bar{F}_{\parallel}\vert_{\phi^*}$. This still remains to be the case when the phase lag is not optimal, as observed through $\Delta\bar{F}_{\parallel}\vert_0$ and $\Delta\bar{F}_{\parallel}\vert_{0.5\pi}$, suggesting that swimmers in a compact phalanx school, such as the $SD = 1L$ school, are more likely to swim past each other due to an imbalance in the net streamwise force. Conversely, the optimal school at $SD = 2L$ has a slightly lower magnitude of $\Delta\bar{F}_{\parallel}\vert_{\phi^*}$ when compared to both optimal $SD = 1L$ and $SD = 3L$ schools. In other words, the most efficient phalanx school, at $SD = 2L$, is able to maintain cohesion effectively, at least in the streamwise direction.

Nevertheless, larger differences in the lateral force of all optimal schools, as captured by $\Delta\bar{F}_{\perp}\vert_{\phi^*}$, suggest that optimal phalanx swimmers would have to direct part of their swimming effort to maintain cohesion in the lateral direction. As one would expect, the magnitude of $\Delta\bar{F}_{\perp}$ is observed to decrease with the separation distance within a phalanx school. For example, the largest observed $\Delta\bar{F}_{\perp}\vert_{\phi^*}$, at an optimum school with $SD = 1L$, is almost 1.25 times larger than of the school with $SD = 2L$. The difference in $\Delta\bar{F}_{\perp}\vert_{\phi^*}$ as a function of SD levels off as the separation distance increases, with little change observed in $\Delta\bar{F}_{\perp}\vert_{\phi^*}$ between $SD = 2L$ and $SD = 3L$. It is worthy to note that $\Delta\bar{F}_{\perp}$ generally shows a strong dependence on the phase lag, ϕ. The largest observed magnitudes of $\Delta\bar{F}_{\perp}$ typically occur during anti-phase motion, with the lowest values occurring during in-phase motion. As in-phase motions also result in a low total work, this suggests an existence of a correlation between stability and the total work.

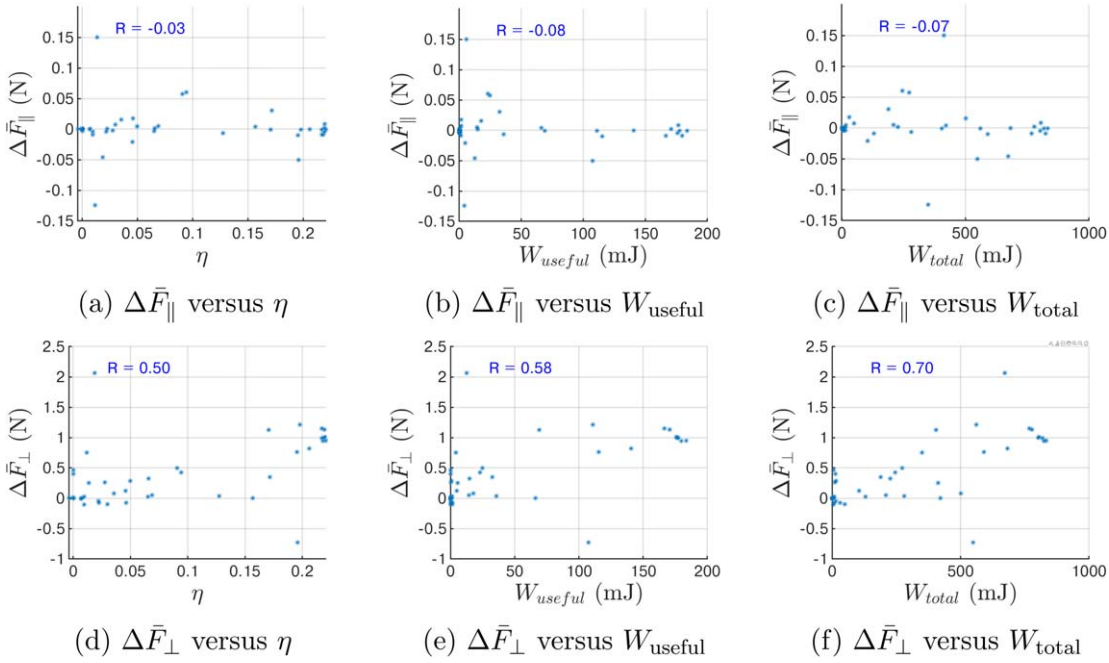

Figure 7. Correlation between stability, efficiency, useful work and total work using the data from $SD = 2L$ case. Top row: net streamwise forces, bottom row: net lateral forces. Correlation coefficient R is included within each image.

To further verify this hypothesis, in figure 7 we present the correlations between the force difference (in both the streamwise and lateral directions) and the efficiency, useful work, and total work taken from the optimization data of $SD = 2L$ case. First, we see that the streamwise force difference is, indeed, significantly lower than the lateral force difference. Additionally, the net streamwise force does not seem to correlate with either of the considered parameters influencing swimming efficiency, although higher values of streamwise instability typically occur for low-efficiency cases. Lateral force difference, on the other hand, correlates the most significantly with the total work (correlation coefficient $R = 0.70$), as predicted. Correlation with useful work is lower, but not insignificant ($R = 0.58$). We see that high-thrust producing configurations (high useful work) do typically result in higher lateral net forces (as occurs, for example, during anti-phase swimming as previously discussed). This results in a net positive correlation between the lateral force difference and efficiency (albeit with a relatively low $R = 0.50$). We remark, however, that the configurations with the highest lateral force differences occur at low efficiencies, the same trend was observed for the streamwise forces.

A strong correlation between stability and total work suggests a relation between stability and energy savings in fish schools, i.e. hydrodynamically stable positions also require a low energy input to maintain. As a low energy input does not necessarily translate into a high thrust and thus a high efficiency, this trend points to an existence of a trade-off between efficient and stable formations of phalanx schools considering variables such as kinematic gaits and phase synchronization.

5. Conclusions

This paper presents an optimization study of accelerating phalanx fish schools considering the midline kinematics, frequency and phase synchronization as optimization parameters, while varying the separation distance within the school to investigate the effect of a school density. A formal optimization procedure allows for a consistent and efficient exploration of the parameter space with the guaranteed convergence to optimum at a specified tolerance. To the authors' knowledge, optimization studies of hydrodynamic interactions in accelerating fish schools have not yet appeared in the literature. The main conclusions of the study can be summarized in the following: (1) An optimum kinematics in a school does not deviate significantly from the optimum kinematics of a solitary swimmer; (2) In-phase and anti-phase motions both show higher efficiency than the phase lag values in between, with the highest efficiency achieved by an anti-phase motion; (3) A separation distance within the school has a profound effect on efficiency: efficiency is decreased in dense schools due to a higher total work required to maintain cohesion, it peaks at an optimum separation distance of about $SD \approx 2L$, and it gradually approaches the efficiency of a solitary swimmer at higher separations. An important conclusion of the current study is that a separation distance has a more profound effect on efficiency than a phase

synchronization; in fact, higher efficiency gains can be attained by varying the separation distance rather than the phase angle in the school; (4) Stability of schooling patterns correlates favorably with the total energy input (hydrodynamically stable positions require low energy input), but not necessarily with efficiency (hydrodynamically stable positions are not necessarily the most efficient), which suggests an existence of trade-off between stable and efficient formations. These insights can be useful for design and control of autonomous bioinspired robotic swarms during acceleration and maneuvers. The presented optimization framework, even with fixed swimmers' positions, partially takes into account the destabilizing effects caused by a difference between the fluid forces acting on the swimmers by penalizing the total work and thus driving the unstable modes away from the optimum solution. However, it does not consider the changes in the background flow that could be incurred were the swimmers allowed to decelerate, accelerate, or diverge from each other. Future work will explore the effects of fully-decoupled motile fish schools on optimum efficiency, and the influence of three-dimensional effects.

We remark that the conclusions of any optimization study are highly sensitive to a definition of the objective function. For example, if one were to choose to maximize the *efficiency* while minimizing the total work, instead of maximizing the *useful work* while minimizing the total work, as considered in the current study, the results could be different. Additionally, the current work does not consider a metabolic energy input of fish required to sustain a given kinematic gait [70–72], which would require coupling of neuromechanical and fluid-structure interaction models of fish, and could be explored in future studies.

Acknowledgments

This work was supported by NSF CMMI-1762827 grant. Computational time was provided by ASU Research Computing Center on the parallel cluster Agave.

Data availability statement

The data that support the findings of this study are available upon reasonable request from the authors.

ORCID iDs

Ahmed Abouhussein https://orcid.org/0000-0001-5423-0555

References

[1] Hemelrijk C, Reid D, Hildenbrandt H and Padding J 2015 The increased efficiency of fish swimming in a school *Fish and Fisheries* **16** 511–21
[2] Herskin J and Steffensen J 1998 Energy savings in sea bass swimming in a school: measurements of tail beat frequency and oxygen consumption at different swimming speeds *Journal of Fish Biology* **53** 366–76
[3] Johansen J, Vaknin R, Steffensen J and Domenici P 2010 Kinematics and energetic benefits of schooling in the labriform fish, striped surfperch embiotoca lateralis *Marine Ecology Progress Series* **420** 221–9
[4] Raspa V, Godoy-Diana R and Thiria B 2013 Topology-induced effect in biomimetic propulsive wakes *J. Fluid Mech.* **729** 377–87
[5] Godoy-Diana R, Vacher J, Raspa V and Thiria B 2019 On the fluid dynamical effects of synchronization in side-by-side swimmers *Biomimetics* **4** 77
[6] Gazzola M, Chatelain P, Van Rees W M and Koumoutsakos P 2011 Simulations of single and multiple swimmers with non-divergence free deforming geometries *J. Comput. Phys.* **230** 7093–114
[7] Ashraf I, Godoy-Diana R, Halloy J, Collignon B and Thiria B 2016 Synchronization and collective swimming patterns in fish (hemigrammus bleheri) *Journal of the Royal Society Interface* **13** 20160734
[8] Ashraf I, Bradshaw H, Ha T-T, Halloy J, Godoy-Diana R and Thiria B 2017 Simple phalanx pattern leads to energy saving in cohesive fish schooling *Proc. Natl Acad. Sci.* **114** 9599–604
[9] Li G, Kolomenskiy D, Liu H, Thiria B and Godoy-Diana R 2019 On the energetics and stability of a minimal fish school *PLoS One* **14** e0215265
[10] Oza A U, Ristroph L and Shelley M J 2019 Lattices of hydrodynamically interacting flapping swimmers *Phys. Rev.* X **9** 041–024
[11] Li L, Nagy M, Graving J M, Bak-Coleman J, Xie G and Couzin I D 2020 Vortex phase matching as a strategy for schooling in robots and in fish *Nat. Commun.* **11** 1–9
[12] Bergmann M and Iollo A 2011 Modeling and simulation of fish-like swimming *J. Comput. Phys.* **230** 329–48
[13] Dewey P A, Quinn D B, Boschitsch B M and Smits A J 2014 Propulsive performance of unsteady tandem hydrofoils in a side-by-side configuration *Phys. Fluids* **26** 041–903
[14] Maertens A P, Gao A and Triantafyllou M S 2017 Optimal undulatory swimming for a single fish-like body and for a pair of interacting swimmers *J. Fluid Mech.* **813** 301–45
[15] Videler J and Hess F 1984 Fast continuous swimming of two pelagic predators, saithe (pollachius virens) and mackerel (scomber scombrus): a kinematic analysis *J. Exp. Biol.* **109** 209–28
[16] Verma S, Novati G and Koumoutsakos P 2018 Efficient collective swimming by harnessing vortices through deep reinforcement learning *Proc. Natl Acad. Sci.* **115** 5849–54

[17] Akanyeti O, Putney J, Yanagitsuru Y R, Lauder G V, Stewart W J and Liao J C 2017 Accelerating fishes increase propulsive efficiency by modulating vortex ring geometry *Proc. Natl Acad. Sci.* **114** 13828–33
[18] Tytell E D 2004 Kinematics and hydrodynamics of linear acceleration in eels, anguilla rostrata *Proceedings of the Royal Society of London. Series B: Biological Sciences* **271** 2535–40
[19] Wise T N, Schwalbe M A and Tytell E D 2018 Hydrodynamics of linear acceleration in bluegill sunfish, lepomis macrochirus *J. Exp. Biol.* **221** jeb190892
[20] Thandiackal R, White C H, Bart-Smith H and Lauder G V 2021 Tuna robotics: hydrodynamics of rapid linear accelerations *Proceedings of the Royal Society* B **288** 20202726
[21] Bergstra J, Bardenet R, Bengio Y and Kégl B 2011 Algorithms for hyperparameter optimization *Advances in Neural Information Processing Systems* **24** 2546–54
[22] Liu Y, Chen Y and Cheng J 2009 A comparative study of optimization methods and conventional methods for sampling design in fishery-independent surveys *ICES J. Mar. Sci.* **66** 1873–82
[23] Kern S and Koumoutsakos P 2006 Simulations of optimized anguilliform swimming *J. Exp. Biol.* **209** 4841–57
[24] Kurt M and Moored K W 2018 Flow interactions of two-and three-dimensional networked bio-inspired control elements in an in-line arrangement *Bioinspiration Biomimetics* **13** 045–002
[25] Newbolt J W, Zhang J and Ristroph L 2022 Lateral flow interactions enhance speed and stabilize formations of flapping swimmers *Physical Review Fluids* **7** L061101
[26] Eloy C 2013 On the best design for undulatory swimming *J. Fluid Mech.* **717** 48
[27] Van Rees W M, Gazzola M and Koumoutsakos P 2013 Optimal shapes for anguilliform swimmers at intermediate reynolds numbers *J. Fluid Mech.* **722** R3–1–R3–12
[28] Novati G, Verma S, Alexeev D, Rossinelli D, Van Rees W M and Koumoutsakos P 2017 Synchronisation through learning for two self-propelled swimmers *Bioinspiration Biomimetics* **12** 036–001
[29] Zhu Y, Pang J-H, Gao T and Tian F-B 2022 Learning to school in dense configurations with multi-agent deep reinforcement learning *Bioinspiration Biomimetics* **18** 015003
[30] Bao Y *et al* 2017 Dynamic interference of two anti-phase flapping foils in side-by-side arrangement in an incompressible flow *Phys. Fluids* **29** 033–601
[31] Yu H, Lu X-Y and Huang H 2021 Collective locomotion of two uncoordinated undulatory self-propelled foils *Phys. Fluids* **33** 011–904
[32] Li L, Ravi S, Xie G and Couzin I D 2021 Using a robotic platform to study the influence of relative tailbeat phase on the energetic costs of side-by-side swimming in fish *Proceedings of the Royal Society* A **477** 20200810
[33] Pan Y and Dong H 2022 Effects of phase difference on hydrodynamic interactions and wake patterns in high-density fish schools *Phys. Fluids* **34** 111–902
[34] Abouhussein A and Peet Y T 2022 Computational framework for efficient highfidelity optimization of bio-inspired propulsion and its application to accelerating swimmers *J. Comput. Phys.* Under Review
[35] Partridge B L 1982 The structure and function of fish schools *Sci. Am.* **246** 114–23
[36] Pavlov D S and Kasumyan A O 2000 Patterns and mechanisms of schooling behavior in fish: a review *Journal of Ichthyology* **40** S163
[37] Ouellette N T and Gordon D M 2021 Goals and limitations of modeling collective behavior in biological systems *Frontiers in Physics* **9** 687–823
[38] Pan Y and Dong H 2020 Computational analysis of hydrodynamic interactions in a high-density fish school *Phys. Fluids* **32** 121–901
[39] Du R, Li Z, Youcef-Toumi K and y Alvarado P V 2015 *Robot Fish: bio-Inspired Fishlike Underwater Robots* (Springer)
[40] Valdivia y Alvarado P P A 2007 Design of biomimetic compliant devices for locomotion in liquid environments *Ph.D. Dissertation* (Massachusetts Institute of Technology)
[41] Xu Y and Peet Y T 2018 Optimum gaits of 2D thunniform locomotion for efficient swimming and performance of fish pair, AIAA Paper 2018-2915 *XXIV AIAA Computational Fluid Dynamics Conference, Atlanta, GA*
[42] Lighthill M 1960 Note on the swimming of slender fish *J. Fluid Mech.* **9** 305–17
[43] Barrett D, Triantafyllou M, Yue D, Grosenbaugh M and Wolfgang M 1999 Drag reduction in fish-like locomotion *J. Fluid Mech.* **392** 183–212
[44] Donley J M and Dickson K A 2000 Swimming kinematics of juvenile kawakawa tuna (euthynnus affinis) and chub mackerel (scomber japonicus) *J. Exp. Biol.* **203** 3103–16
[45] Bergmann M, Iollo A and Mittal R 2014 Effect of caudal fin flexibility on the propulsive efficiency of a fish-like swimmer *Bioinspiration Biomimetics* **9** 046–001
[46] Borazjani I and Sotiropoulos F 2010 On the role of form and kinematics on the hydrodynamics of self-propelled body/caudal fin swimming *J. Exp. Biol.* **213** 89–107
[47] Ho L W and Legendre A 1989 spectral element method for simulation of incompressible unsteady viscous free-surface flows *Ph.D. Dissertation* Massachusetts Institute of Technology
[48] Deville M O, Fischer P F and Mund E 2002 *High-Order Methods for Incompressible Fluid Flow* (Cambridge University Press)
[49] Maday Y and Patera A T 1989 Spectral element methods for the incompressible Navier-Stokes equations, in State-of-the-art surveys on computational mechanics (A90-47176 21-64.) *American Society of Mechanical Engineers* (New York:) pp 71–143
[50] Aitken A C 1927 On Bernoulli's numerical solution of algebraic equations *Proceedings of the Royal Society of Edinburgh* **46** 289–305
[51] Causin P, Gerbeau J-F and Nobile F 2005 Added-mass effect in the design of partitioned algorithms for fluid-structure problems *Comp. Methods Appl. Mech. Eng.* **194** 4506–27
[52] F¨orster C, Wall W A and Ramm E 2007 Artificial added mass instabilities in sequential staggered coupling of nonlinear structures and incompressible viscous flows *Comp. Methods Appl. Mech. Eng.* **196** 1278–93
[53] Daghooghi M and Borazjani I 2015 The hydrodynamic advantages of synchronized swimming in a rectangular pattern *Bioinspiration Biomimetics* **10** 056–018
[54] Abouhussein A, Islam N and Peet Y T 2022 Constraint enforcement to guarantee strictly feasible solutions in a surrogate based optimizer, AIAA Paper 2022-1611 *AIAA SciTech Forum and Exposition, San Diego, CA*
[55] Marler R T and Arora J S 2004 Survey of multi-objective optimization methods for engineering *Structural and Multidisciplinary Optimization* **26** 369–95
[56] Webb P W 1975 Hydrodynamics and energetics of fish propulsion *Bulletin-Fisheries Research Board of Canada* **190** 1–159
[57] Tytell E D and Lauder G V 2004 The hydrodynamics of eel swimming: I. Wake structure *J. Exp. Biol.* **207** 1825–41
[58] McKay M D, Beckman R J and Conover W J 1979 Comparison of three methods for selecting values of input variables in the analysis of output from a computer code *Technometrics* **21** 239–45

[59] Bainbridge R 1958 The speed of swimming of fish as related to size and to the frequency and amplitude of the tail beat *J. Exp. Biol.* **35** 109–33
[60] Triantafyllou M S, Triantafyllou G and Yue D 2000 Hydrodynamics of fishlike swimming *Annu. Rev. Fluid Mech.* **32** 33–53
[61] Maertens A, Triantafyllou M S and Yue D K 2015 Efficiency of fish propulsion *Bioinspiration Biomimetics* **10** 046–013
[62] Shadwick R E, Katz S L, Korsmeyer K E, Knower T and Covell J W 1999 Muscle dynamics in skipjack tuna: timing of red muscle shortening in relation to activation and body curvature during steady swimming *J. Exp. Biology* **202** 2139–50
[63] Di Santo V *et al* 2021 Convergence of undulatory swimming kinematics across a diversity of fishes *Proc. Natl Acad. Sci.* **118** e2113206118
[64] Li N, Liu H and Su Y 2017 Numerical study on the hydrodynamics of thunniform bio-inspired swimming under self-propulsion *PLoS One* **12** e0174740
[65] Knower T, Shadwick R E, Katz S L, Graham J B and Wardle C S 1999 Red muscle activation patterns in yellowfin (thunnus albacares) and skipjack (katsuwonus pelamis) tunas during steady swimming *J. Exp. Biol.* **202** 2127–38
[66] Shadwick R E and Syme D A 2008 Thunniform swimming: muscle dynamics and mechanical power production of aerobic fibres in yellowfin tuna (thunnus albacares) *J. Exp. Biol.* **211** 1603–11
[67] Fish F E 1996 Transitions from drag-based to lift-based propulsion in mammalian swimming *Am. Zool.* **36** 628–41
[68] Vogel S 2008 Modes and scaling in aquatic locomotion *Integr. Comp. Biol.* **48** 702–12
[69] Weihs D 1973 Hydromechanics of fish schooling *Nature* **241** 290–1
[70] Killen S S, Marras S, Steffensen J F and McKenzie D J 2012 Aerobic capacity influences the spatial position of individuals within fish schools *Proceedings of the Royal Society B: Biological Sciences* **279** 357–64
[71] Burgerhout E, Tudorache C, Brittijn S A, Palstra A P, Dirks R P and van den Thillart G E E J M 2013 Schooling reduces energy consumption in swimming male European eels, Anguilla anguilla L. *J. Exp. Mar. Biol. Ecol.* **448** 66–71
[72] Xargay E, Burton K and Shorter K 2019 A low-order model of dolphin swimming dynamics: fluke flexibility and energetics *Proceedings of the XXII Biennial Conference on the Biology of Marine Mammals, Barcelona, Spain*